Microfluid Nanofluid (2013) 14:895–902
DOI 10.1007/s10404-012-1120-6

SHORT COMMUNICATION

Microscale confinement features can affect biofilm formation

Aloke Kumar · David Karig · Rajesh Acharya · Suresh Neethirajan · Partha P. Mukherjee · Scott Retterer · Mitchel J. Doktycz

Received: 22 August 2012 / Accepted: 28 November 2012 / Published online: 19 December 2012

Abstract The majority of bacteria in nature live in biofilms, where they are encased by extracellular polymeric substances (EPS) and adhere to various surfaces and interfaces. Investigating the process of biofilm formation is critical for advancing our understanding of microbes in their most common mode of living. Despite progress in characterizing the effect of various environmental factors on biofilm formation, work remains to be done in the realm of exploring the inter-relationship between hydrodynamics, microbial adhesion and biofilm growth. We investigate the impact of secondary flow structures, which are created due to semi-confined features in a microfluidic device, on biofilm formation of *Shewanella oneidensis* MR-1. Secondary flows are important in many natural and artificial systems, but few studies have investigated their role in biofilm formation. To direct secondary flows in the creeping flow regime, where the Reynolds number is low, we flow microbe-laden culture through microscale confinement features. We demonstrate that these confinement features can result in pronounced changes in biofilm dynamics as a function of the fluid flow rate.

Keywords Microfluidics · Biofilms · Secondary flows · Bacteria · Micro-vortices

1 Introduction

Biofilms are highly organized and complex aggregates of microbes that are encased by extracellular polymeric substances (EPS) and provide significant resistance of the constituent microbes to external stresses (Costerton et al. 1995; Haussler and Parsek 2010; Remis et al. 2010; Wong and O'Toole 2011). Biofilms can be harmful or advantageous, depending on the nature of the situation. For example, in applications such as microbial fuel cells, biofilms growing over an electrode surface can lead to current generation (Lovley 2008; Qian et al. 2009; Nealson and Finkel 2011). On the other hand, biofilms lead to persistent infections in humans and fouling in applications such as water treatment and oil pipelining (Callow and Callow 2011; Chai et al. 2011; Khoo and Grinstaff 2011; Shrout et al. 2011; Wong and O'Toole 2011). The ubiquity of biofilms and their ability to resist external stresses make them relevant to a variety of applications and problems. Thus, developing a deeper understanding of the forces driving biofilm formation is a problem of great importance. However, biofilm formation is a complex, multi-scale process that is mediated by several factors such as environmental factors (e.g., hydrodynamics), cell-to-cell communication and cell phenotype changes (Stewart and Franklin 2008). The use of microfluidic devices is emerging as a useful

Electronic supplementary material The online version of this article (doi:10.1007/s10404-012-1120-6) contains supplementary material, which is available to authorized users.

A. Kumar (✉) · R. Acharya · S. Retterer · M. J. Doktycz
Biosciences Division, Oak Ridge National Laboratory, Oak Ridge, TN, USA
e-mail: kumara1@ornl.gov

D. Karig
Research and Exploratory Development Department, Johns Hopkins University Applied Physics Laboratory, Baltimore, MD, USA

S. Neethirajan
School of Engineering, University of Guelph, Guelph, ON N1G 2W1, Canada

P. P. Mukherjee
Department of Mechanical Engineering, Texas A&M University, College Station, TX, USA

approach to elucidate key determinants of biofilm formation dynamics (Neethirajan et al. 2012). Accordingly, we focus on harnessing microfluidic devices to quantify the effects of hydrodynamics on *Shewanella oneidensis* MR-1 biofilm formation.

Biofilms often grow in flowing or stationary liquid systems, and in such systems, hydrodynamic effects such as shear stress and mass transport have profound ramifications (Ardekani and Gore 2012; Liu and Tay 2002; Mabrouk et al. 2010; Paramonova et al. 2009; Purevdorj et al. 2002; Stoodley et al. 1999). For example, hydrodynamics can influence cell attachment and detachment processes, regulation of EPS production, and transport of signaling molecules. Recently, several investigations have used microfluidic devices to quantify the impact of hydrodynamics and mass transport on these processes (Nakagaki et al. 2000; Cho et al. 2007; De la Fuente et al. 2007; Richter et al. 2007; Ingham and Vlieg 2008; Lee et al. 2008; Volfson et al. 2008; Boedicker et al. 2009; Hohne et al. 2009; Janakiraman et al. 2009; Chen et al. 2010; Connell et al. 2010; Kim et al. 2010; Yawata et al. 2010; Park et al. 2011), yet several important effects remain to be characterized. In particular, secondary flow structures are an aspect of hydrodynamics that can exhibit rich dynamics, but their role in biofilm formation has been sparsely studied. Rusconi et al. (2010) examined suspended filamentous biofilms (streamers) in a curved microfluidic device and showed that secondary flow structures can cause the formation of narrow streams of bacteria. Subsequent studies have demonstrated the origins and further relevance of hydrodynamics and flow structures to biomass accumulation and streamer structures (Guglielmini et al. 2011; Rusconi et al. 2011; Valiei et al. 2012). However, many consequences of secondary flow structures remain to be characterized.

In this communication, we study a previously uncharacterized hydrodynamical effect—the role of secondary flow structures resulting from semi-confined geometric features. A microfluidic device with semi-confined structures (Fig. 1) is used for investigating biofilm formation of the microbe *S. oneidensis* MR-1. *S. oneidensis* MR-1 is a metal reducing bacterium of interest for several bioremediation and energy applications (Lovley 2008) that is also well known for its biofilm forming abilities (Thormann et al. 2004). The time-evolution dynamics of *S. oneidensis* biofilms are studied and quantified in the baffled devices using epifluorescence microscopy. The features in our microfluidic device are inspired by mesoscopic features that can be found on shark skins (Fig. 5a, b of Callow and Callow 2011). Shark skin contains mesoscopic topographic features, which are believed to aid in anti-fouling ability (Callow and Callow 2011). Inclined baffle structures (Fig. 1) serve as the semi-confined features on the device, and these features are the bio-inspired region of our device. Our findings indicate that such features can be utilized to delay biofilm development through hydrodynamics.

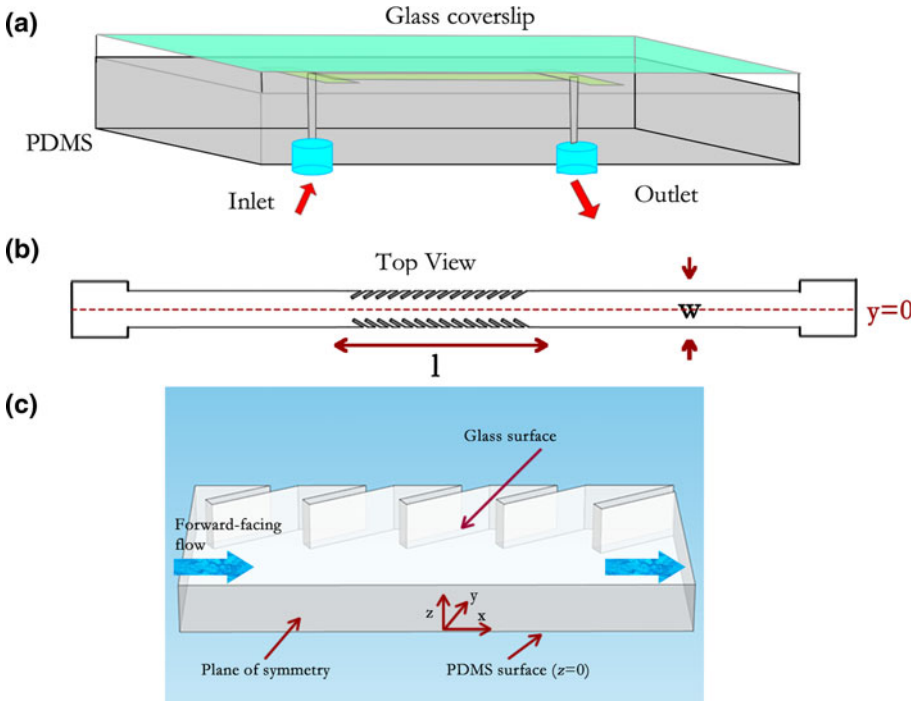

Fig. 1 **a** Schematic of the microfluidic setup. **b** *Top view* layout of the portion of channel showing the regions with baffles. **c** 3D schematic of the device. The PDMS surface serves as the image plane

2 Experimental methods

2.1 Bacterial cultivation

The GFP expressing *S. oneidensis* MR-1 wild type used here has been described previously (Thormann et al. 2004) (strain AS93). Cultures were prepared by inoculating from a −80 °C stock and growing overnight in LB broth in a shaking incubator at 30 °C. A dilute microbial suspension was created by mixing 5 mL of LB media with 150 µL of culture. The resulting solution had an optical density of 0.1 (at 415 nm).

2.2 Microfluidics and data acquisition

Various microfabrication processes were employed to realize the microfluidic device (Fig. 2). First, a silicon (Si) wafer is coated with positive photoresist (SPR 220) and spun till the resist thickness is 7 µm. The resist was given an initial soft bake to harden the resist. Using a mask, the wafer was exposed to UV radiation. The wafer was placed in developer allowing the exposed features to dissolve, leaving only features which were opaque in the mask (Fig. 2a, b).

The developed wafer was etched with reactive ion etching (RIE). High energy ions from the plasma process bombard the wafer and displace silicon ions. This process has a high selectivity for Si ions over the photoresist, at a rate of 1:50 photoresist to silicon etch depth. After etching, the wafer was treated to a hot resist strip bath to remove any remaining photoresist on the wafer (Fig. 2c, d). This wafer served as the Si master.

The microfluidic channels were prepared from polydimethylsiloxane (PDMS, Slygard 184 silicone elastomer kit, Dow Corning) using a Si master (Fig. 1). Each channel was sealed to a glass cover slip (thickness ∼0.17 mm), after 30 s of exposure to an oxygen plasma. To achieve proper sealing, the chip was further subjected to a bake process for 5 min at 75 °C. The device itself has a single inlet and a single outlet. The channel (Fig. 1b) has a width (w) of 450 µm and extends in the z-direction for a height (h) of 125 µm, and contains an axially symmetric, semi-confined region with periodic arrays of baffles on the side walls. Figure 1c shows the three-dimensional architecture of the device. The PDMS baffles are contained between the glass cover slip and the PDMS channel. The baffle geometries are specified by the variables shown in Fig. 3a. The baffle width, β, is fixed at 30 µm. The parameter λ can be interpreted as the baffle pitch and in Fig. 3, its value is 150 µm. Experiments were also conducted by changing the baffle pitch to 100, 200 and 250 µm. The baffle inclination angle θ is 30°. The baffles span a length of 2.5 mm and the length of the entire channel is 2 cm. The microfluidic device was set up inside a 30 °C heated enclosure surrounding the stage area of the fluorescence microscope. The microfluidic device was disinfected using 70 % ethanol for 5 min, followed by rinsing with LB medium to remove ethanol. Subsequently, the inoculum was infused into the channels by means of a syringe pump (Harvard Apparatus). Fluorescent images of biofilm formation were captured on a Zeiss Axioplan 2 microscope with a Diagnostic Instruments Spot Xplorer XS Camera, a Ludl BioPrecision motorized stage, a Till Polychrome IV fluorescent excitation source, and a 10× objective. Higher magnification images were taken using a 40× air objective. Chroma filters were used for GFP imaging with the Till excitation wavelength set at 488 nm. Images were captured every 25 min using the IPLab 4.08 (Scanalytics, Inc.)

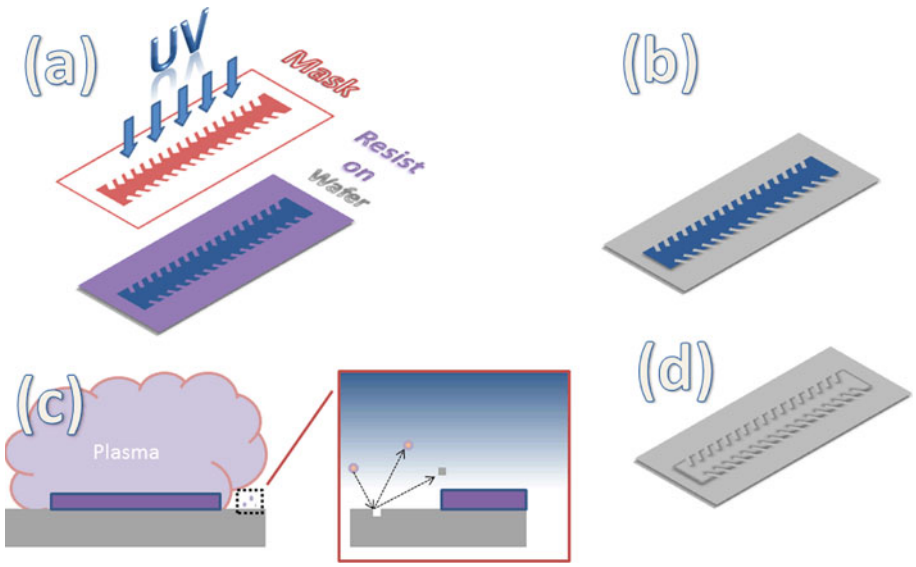

Fig. 2 **a** A mask is placed over the positive resist-coated wafer and a UV light treatment is given. **b** The wafer is placed in a developer solution and parts exposed to UV light will become soluble in developer, therefore leaving only the channel design. **c** The wafer is etched using reactive ion etching (RIE). The process is highly selective to displacing silicon ions 50 times more than it is to displacing resist. This creates the Si mask. **d** Polydimethylsiloxane (PDMS) is mixed and poured over the device and baked till hardened

software package with 2×2 binning and an 80 ms exposure time.

Fluid flow conditions inside the microfluidic device were studied, through both numerical computations and experimental velocity measurements. For numerical computations, the software package Comsol Multiphysics® (Boston, MA) was utilized. Numerical computations for different flow conditions were performed using laminar flow conditions and a volume-averaged approach, thus yielding 2-D flow profiles. Corresponding experimental velocity measurements were performed using the micro-scale particle image velocimetry (μPIV) technique (Santiago et al. 1998). For μPIV analysis, 500 nm red fluorescent particles (Life Technologies, USA) were used as tracers. PIVlab, which is a Matlab® based software package developed by W. Thielicke and E. J. Stamhuis, was used to evaluate images to yield velocity data. A time interval of 0.1 s between consecutive images and an ensemble averaged approach (Wereley et al. 2002) was used to conduct the μPIV analysis (see Supplementary Information).

Bacteria motility on the PDMS surface was studied by taking images of bacteria at 1 frame per second (fps). Using the Mosaic plugin for ImageJ (NIH), we track bacteria in the images based on their size, relative brightness and the number of frames they appear in. After tracking, data are obtained and it is used in conjunction with our Matlab® algorithms to calculate average velocities, qualify movement, and obtain parameters.

3 Results

The intended function of the baffles is to create secondary flows as shown in Fig. 3a. The flow rates employed here correspond to a Reynolds number (Re) between 10^{-3} and 10^{-4}, and at these extremely low Re values, the flow is in the creeping flow (linear) regime. The values quoted above, refer to a local Reynolds number defined as

$$Re = \frac{U\delta \sin\,\theta}{v}$$

where U refers to the average velocity in the channel, $\delta \sin\theta$ is the depth of the channel (along y-axis) and v is the kinematic viscosity of the liquid medium. This definition of the local Reynolds number is adapted from Shen and Floryan (1985). Figure 3a depicts a numerical simulation of creeping flow across two baffles and shows how these baffles divide the flow into two distinct regions. The secondary flow region consists of a set of vortices and can be visualized through the closed streamlines in the region between the two baffles. These vortex structures depend strongly on the geometric structure of the baffles, viz., angle of inclination and the aspect ratio. Outside of this region, the flow consists of open streamlines. These two regions are separated by the separatrix (the separating streamline). Figure 3b depicts the vortex structure using velocity vectors obtained through a μPIV analysis of experimental images (see also Supplementary Video 1). Such flow separation in semi-confined regions is a profoundly interesting feature for several reasons (Moffatt 1964; Shen and Floryan 1985; Wierschem and Aksel 2004), one of them being that it can cause low mass transfer between primary and secondary flow regions (Wierschem and Aksel 2004).

To explore the role of secondary flows, microbial solution was allowed to flow through the microfluidic device at a constant rate for a period of several hours. The flow of microbe-laden fluid in the microfluidic device can take place in two modes: forward-facing mode and backward-facing mode. In the forward-facing mode, the baffles face the oncoming flow (Fig. 1c), and face away from the flow in the backward-facing mode. We will first discuss

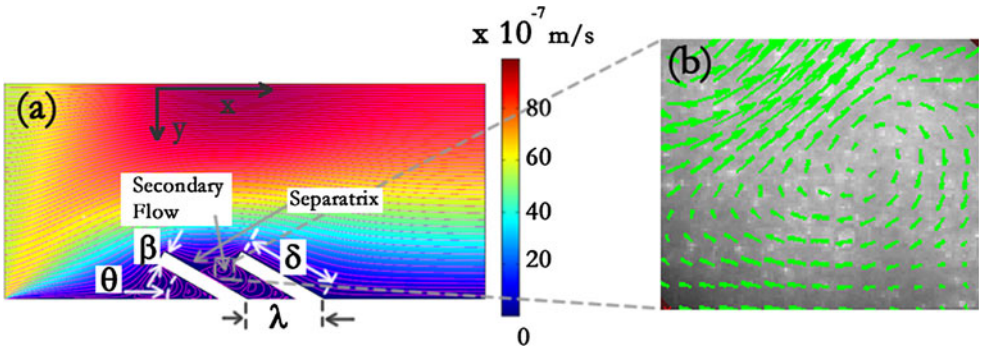

Fig. 3 Secondary flow in the microfluidic device. **a** The baffle pitch (λ) is 150 μm and it has an inclination angle (θ) of 150°. The baffle width (β) is 30 μm and δ is 200 μm. Fluid enters from the *left* at a flow rate of 0.8 μL/h. Depth-averaged numerical simulations yielded the *contour plot* representing velocity in m/s and streamlines are also shown. The separatrix is the streamline separating the primary and secondary flow regions. The baffles lead to the formation of secondary flows (micro-vortices) in the inter-baffle region. **b** PIV analysis of experimental images taken near the PDMS surface depicts one of the vortices that comprise the secondary flow region through velocity vectors (*green*) (color figure online)

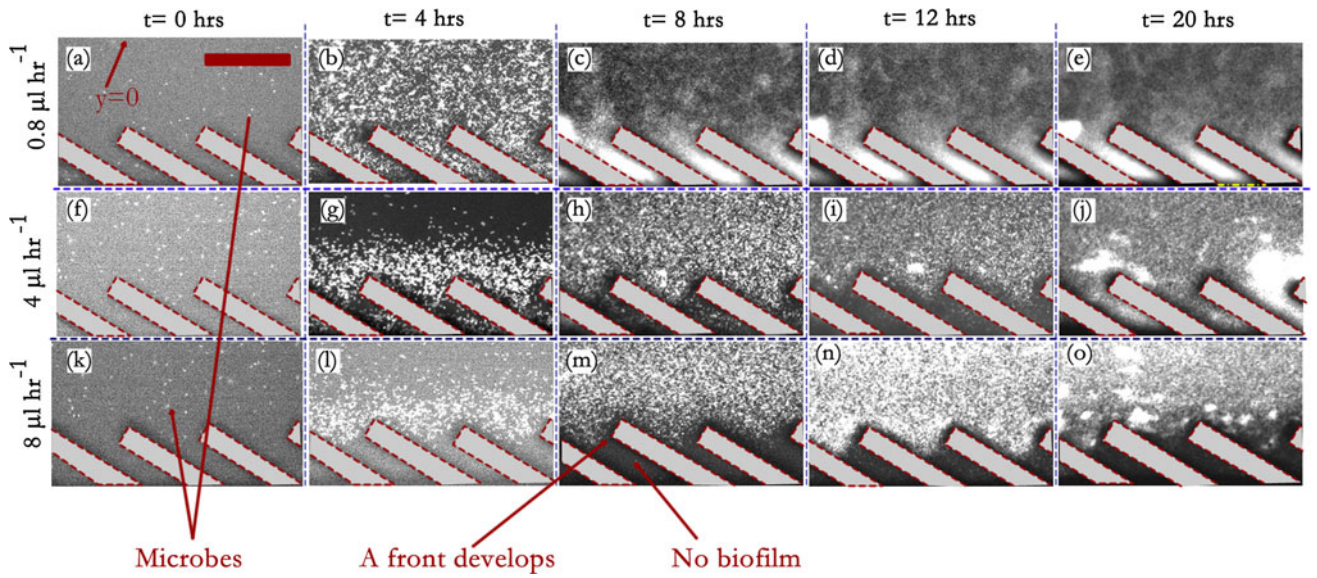

Fig. 4 Time-evolution of the biofilm at different flow rates. The PDMS surface serves as the image plane (refer to Fig. 1c). **a–e** Image series corresponds to a flow rate of 0.8 µL h^{-1}. **f–j** Image series corresponds to a flow rate of 4 µL h^{-1}. **k–o** Image series corresponds to a flow rate of 8 µL h^{-1}

results with regards to forward-facing flows and then discuss results with respect to backward-facing flows.

Figure 4a–o depicts time-series data of biofilm formation on the PDMS surface at different flow rates. The baffle pitch is 150 µm. Since the device is axially ($y = 0$) symmetric, Fig. 4a–o only shows half of the device. At the low flow rate of $f = 8 \times 10^{-1}$ µL h^{-1} ($Re \sim 4 \times 10^{-4}$), the microbes are dispersed approximately uniformly in the main channel and in the confinement regions. Figure 4a is a snapshot at $t = 0$ h, and fluorescent microbes can be seen against a darker background. At this low optical magnification, each microbial cell spans only a few pixels. After a period of only 4 h (Fig. 4b), small colonies initiate at various regions of the PDMS surface ($z = 0$) and finally the biofilm covers the entire device (Fig. 4c–e). The biofilm forms a thin film on the PDMS surface, which extends a few microns in the z-direction (typical height <10 µm) (Supplementary Fig. 1). While the individual microbes can be seen on the PDMS surface in Fig. 4a, the colonies can be seen in Fig. 4b, and in Fig. 4c–e, the biofilm can be seen to cover the entire device. Higher magnification images reveal the distinct patterns of microbial growth, and it was estimated that the cell doubling time of the microbe is approximately 40 ± 10 min (Supplementary Fig. 2).

When experiments were conducted at a much higher flow rate ($f = 4$ µL h^{-1}, $Re \sim 2 \times 10^{-3}$), distinct changes in biofilm formation dynamics and morphology were observed. For forward-facing flow, microbial adhesion was confined primarily to the non-baffled central region of the channel, as indicated by the relative brightness of this region in Fig. 4f–j. As the flow rate was increased to $f = 8$ µL h^{-1} ($Re \sim 4 \times 10^{-3}$), this change in the spatial distribution of microbes becomes more prominent. Specifically, the microbes can be seen accumulating in the form of a front near the baffle tips. At the lowest flow rate condition, microbes colonize all sections of the device by $t = 8$ h (Fig. 4c), whereas a distinctly different distribution of microbes is noticed in the higher flow rate condition (Fig. 4m) (see Supplementary Fig. 3). Biofilm formation occurs in the region external to the baffles and is bordered by this front near the baffle regions. This front (Fig. 4n) delineates the region where biofilm formation occurs, and the region where biofilm formation does not occur (see Supplementary Video 2). At this flow rate, even after 20 h biofilm formation did not occur inside the inter-baffle region (Fig. 4o). When the higher flow rate experiment ($f = 8$ µL h^{-1}) is repeated with the flow direction being reversed (backward-facing flow), biofilm morphologies are qualitatively similar to those obtained with the forward-facing flow (Fig. 5a). This can be expected as in this low Re regime, reversing the flow leads to an identical flow structure (i.e., streamlines remain unaltered).

Till now, we have studied biofilm formation dynamics as a function of fluid flow, by changing the volume flow rates and reversing its direction. Another, important variable that impacts biofilm formation dynamics is the baffle geometry. If, the baffle pitch is increased (keeping the inclination angle constant) then biofilm formation dynamics changes. This is depicted in Fig. 5b, c. In Fig. 5b, the baffle pitch is 250 µm. Here even at the higher flow rate ($f = 8$ µL h^{-1}), biofilm formation can be observed inside the inter-baffle region. To make a more quantitative

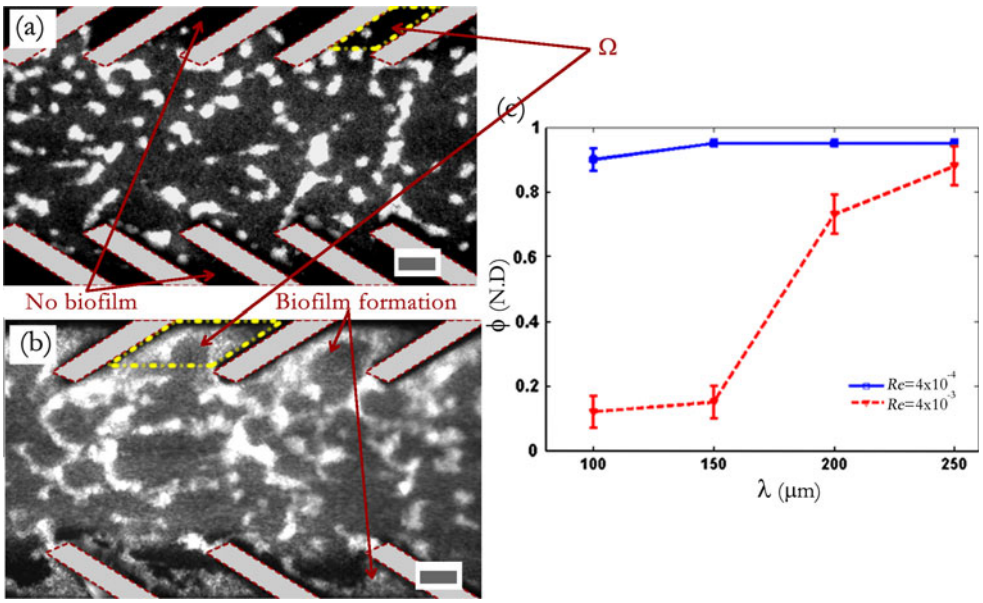

Fig. 5 Biofilm formation at a flow rate of 8 μL h^{-1}. **a** Biofilm formation in with backflow. **b** A different baffle design with a higher pitch. In this case, biofilm formation occurs in the inter-baffle region as well. **c** Surface coverage values in the inter-baffle region for two flow conditions at 20 h as a function of baffle pitch. The inter-baffle region for **a** and **b** is demarcated by *dashed yellow lines* and is denoted as Ω (color figure online)

assessment, we introduce a parameter—surface coverage (ϕ). To calculate this, we first delineate the inter-baffled regions (Ω) (Fig. 5a, b). If the image corresponding to inter-baffled regions consists of $m \times n$ pixels, a corresponding phase matrix, $P(i, j)$, is defined such that

$$P(i,j) = \begin{cases} 0 & \text{if } (i,j) \text{ is not occupied by bacteria} \\ 1 & \text{otherwise} \end{cases} \quad \exists\, i \le m, j \le n \tag{1}$$

The non-dimensional surface coverage is the probability that a pixel is occupied by bacteria, and is given by

$$\phi(\Omega) = \bar{P} \tag{2}$$

Lower values of ϕ denote that less surface is occupied by the microbes. The variation of ϕ (measured after 20 h) with baffle pitch and flow rates is shown in Fig. 5c.

4 Discussion

Our experiments simulate conditions where there is a constant flow of bacteria-laden liquid across a semi-confined feature. It is also important to note that unlike some investigations which have explored the role of topographic features on biofilm formation (Chung et al. 2007; Hochbaum and Aizenberg 2010), the feature sizes of our baffle device are significantly larger than the length scale of the microbe.

Fluid flow rate impacts biofilm formation in our device by affecting the spatial distribution of microbes. The general flow characteristic for all flow rates examined in our experiments are described in Fig. 3. As the flow rate is increased, flow velocity simply scales linearly. Thus, studying biofilm formation for different flow rates allows us to explore the relative contributions of hydrodynamics versus cell behavior such as motility. Specifically, comparison of time scales of various events provides us with an understanding of how change of flow rate in these low Reynolds number regimes can affect biofilm formation. The microbes have their own motion (Brownian motion, twitching motility, etc) and an associated characteristic surface velocity. Apart from their own motion, fluid advection is another component of microbial transport. The ratios of the characteristic surface velocities of the microbes and characteristic fluid velocity ($\tau = v_{\text{microbe}}/v_{\text{fluid}}$) provides a measure of the relative importance of microbial motion dominated transport to fluidic advection. The characteristic surface velocity of the microbial strain used here can be determined experimentally. Using particle tracking for microbes near the PDMS surface, we measured velocities of the microbes under no flow conditions. The results are shown in Fig. 6. Figure 6 provides an estimate of v_{microbe}. Since we are interested in the behavior near the baffles, estimate of v_{fluid} is provided by the velocity along the separating streamline (rather than U). This can be estimated from numerical simulations (Fig. 3a). For the baffle with $\lambda = 150$ μm (Fig. 4), at the low flow rate condition (8×10^{-1} μL h^{-1}), the average flow velocity in the device is comparable to the surface associated motion of the microbes and $\tau = O(1)$. Thus, at the low flow rate condition, microbial motion and advection both contribute to the microbial distribution on the surface. Microbial motion allows the bacteria to enter into the inter-baffle region (Ω), thus allowing it to colonize that area. At higher flow rates (8 μL h^{-1}) $\tau = O(10)$, and

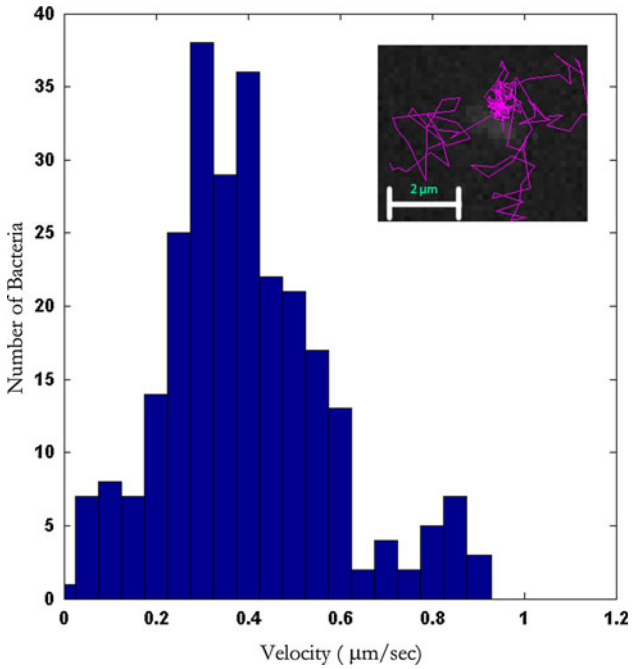

Fig. 6 Movement of over 200 bacterial tracks on the PDMS surface was tracked. The velocity histogram is depicted. *Inset* representative track of one bacteria tracked for over 60 s

fluidic advection dominates transport. Fluidic advection causes the microbes to preferentially stay in the primary flow region, leading to the stepped biofilm profile that we see in Fig. 4n. When the baffle pitch is increased (Fig. 5b), the separatrix enters into the semi-confined region (where fluid velocities are lower) (Shen and Floryan 1985), and τ decreases even at the higher flow rates (8 μL h^{-1}), allowing microbes to colonize the inter-baffle region. Thus, advection dominated transport in conjunction with a low mass transfer between primary and a secondary flow contributes to the development of the 'front formation' phenomenon that we observed.

However, several other factors make the above discussed results both complex and interesting. For example, increased flow rates also have concurrent physiological effects on microbes. Higher flow rates (or equivalently higher shear rates) lead to high EPS production (see Supplementary Fig. 4). The coupling of the various biological processes and fluid flow is not fully understood and detailed investigations are currently underway, where we are investigating the effect of fluid flow on attachment times and EPS production.

5 Conclusions

In summary, we have shown that secondary flow structures arising due to microscale semi-confinement features can affect biofilm formation as a function of the flow velocity. We found that, under certain conditions, biofilm formation inside the confinement regions was delayed significantly. Biofilm formation inside these features is also a function of the geometry of the confinement regions. The demonstration of the effect of semi-confined features on biofilm formation offers new opportunities for developing hydrodynamic approaches for biofilm control. As discussed previously, biofilms can be beneficial or detrimental. Accordingly, in some applications, our findings can be utilized for designing devices where biofilm formation can be directed. In other applications, these results can be utilized for designing of non-fouling surfaces.

Acknowledgments The authors would like to thank Dr. Alfred Spormann at Stanford University for providing the bacterial strains. A. Kumar performed the work as a Eugene P. Wigner Fellow at the Oak Ridge National Laboratory (ORNL). A portion of this research was conducted at the Center for Nanophase Materials Sciences, which is sponsored at ORNL by the Scientific User Facilities Division, US Department of Energy (US DOE). The authors acknowledge research support from the US DOE Office of Biological and Environmental Sciences. ORNL is managed by UT-Battelle, LLC, for the US DOE under contract no. DEAC05-00OR22725. The authors also acknowledge the Natural Sciences and Engineering Research Council of Canada for providing NSERC fellowship to Dr. Neethirajan.

References

Ardekani AM, Gore E (2012) Emergence of a limit cycle for swimming microorganisms in a vortical flow of a viscoelastic fluid. Phys Rev E 85(5):056309. doi:10.1103/PhysRevE.85.056309

Boedicker JQ, Vincent ME, Ismagilov RF (2009) Microfluidic confinement of single cells of bacteria in small volumes initiates high-density behavior of quorum sensing and growth and reveals its variability. Angewandte Chemie 48(32):5908–5911. doi:10.1002/anie.200901550

Callow JA, Callow ME (2011) Trends in the development of environmentally friendly fouling-resistant marine coatings. Nat Commun 2:244. doi:10.1038/ncomms1251

Chai L, Vlamakis H, Kolter R (2011) Extracellular signal regulation of cell differentiation in biofilms. MRS Bull 36(5):374–379. doi:10.1557/mrs.2011.68

Chen CH, Lu Y, Sin MLY, Mach KE, Zhang DD, Gau V, Liao JC, Wong PK (2010) Antimicrobial susceptibility testing using high surface-to-volume ratio microchannels. Anal Chem 82(3):1012–1019. doi:10.1021/ac9022764

Cho HJ, Jonsson H, Campbell K, Melke P, Williams JW, Jedynak B, Stevens AM, Groisman A, Levchenko A (2007) Self-organization in high-density bacterial colonies: efficient crowd control. PLoS Biol 5(11):2614–2623. doi:e30210.1371/journal.pbio.0050302

Chung KK, Schumacher JF, Sampson EM, Burne RA, Antonelli PJ, Brennan AB (2007) Impact of engineered surface microtopography on biofilm formation of Staphylococcus aureus. Biointerphases 2(2):89–94. doi:10.1116/1.2751405

Connell JL, Wessel AK, Parsek MR, Ellington AD, Whiteley M, Shear JB (2010) Probing prokaryotic social behaviors with bacterial "Lobster Traps". Mbio 1(4):e00202–e00210. doi:1128/mBio.00202-10

Costerton JW, Lewandowski Z, Caldwell DE, Korber DR, Lappinscott HM (1995) Microbial biofilms. Annu Rev Microbiol 49:711–745

De la Fuente L, Montanes E, Meng YZ, Li YX, Burr TJ, Hoch HC, Wu MM (2007) Assessing adhesion forces of type I and type IV pili of Xylella fastidiosa bacteria by use of a microfluidic flow chamber. Appl Environ Microbiol 73(8):2690–2696. doi:101128/Aem.02649-06

Guglielmini L, Rusconi R, Lecuyer S, Stone HA (2011) Three-dimensional features in low-Reynolds-number confined corner flows. J Fluid Mech 668:33–57. doi:10.1017/s0022112010004519

Haussler S, Parsek MR (2010) Biofilms 2009: new perspectives at the heart of surface-associated microbial communities. J Bacteriol 192(12):2941–2949. doi:10.1128/jb.00332-10

Hochbaum AI, Aizenberg J (2010) Bacteria pattern spontaneously on periodic nanostructure arrays. Nano Lett 10(9):3717–3721. doi:10.1021/nl102290k

Hohne DN, Younger JG, Solomon MJ (2009) Flexible microfluidic device for mechanical property characterization of soft viscoelastic solids such as bacterial biofilms. Langmuir 25(13):7743–7751. doi:10.1021/la803413x

Ingham CJ, Vlieg J (2008) MEMS and the microbe. Lab Chip 8(10):1604–1616. doi:10.1039/b804790a

Janakiraman V, Englert D, Jayaraman A, Baskaran H (2009) Modeling growth and quorum sensing in biofilms grown in microfluidic chambers. Ann Biomed Eng 37(6):1206–1216. doi:10.1007/s10439-009-9671-8

Khoo X, Grinstaff MW (2011) Novel infection-resistant surface coatings: a bioengineering approach. MRS Bull 36(5):357–366. doi:10.1557/mrs.2011.66

Kim KP, Kim YG, Choi CH, Kim HE, Lee SH, Chang WS, Lee CS (2010) In situ monitoring of antibiotic susceptibility of bacterial biofilms in a microfluidic device. Lab Chip 10(23):3296–3299. doi:10.1039/c0lc00154f

Lee JH, Kaplan JB, Lee WY (2008) Microfluidic devices for studying growth and detachment of Staphylococcus epidermidis biofilms. Biomed Microdevices 10(4):489–498. doi:10.1007/s10544-007-9157-0

Liu Y, Tay JH (2002) The essential role of hydrodynamic shear force in the formation of biofilm and granular sludge. Water Res 36(7):1653–1665. doi:10.1016/s0043-1354(01)00379-7

Lovley DR (2008) The microbe electric: conversion of organic matter to electricity. Curr Opin Biotechnol 19(6):564–571. doi:10.1016/j.copbio.2008.10.005

Mabrouk N, Deffuant G, Tolker-Nielsen T, Lobry C (2010) Bacteria can form interconnected microcolonies when a self-excreted product reduces their surface motility: evidence from individual-based model simulations. Theory Biosci 129(1):1–13. doi:10.1007/s12064-009-0078-8

Moffatt HK (1964) Viscous and resistive eddies near a sharp corner. J Fluid Mech 18(1):1–18. doi:10.1017/s0022112064000015

Nakagaki T, Yamada H, Toth A (2000) Maze-solving by an amoeboid organism. Nature 407(6803):470. doi:10.1038/35035159

Nealson KH, Finkel SE (2011) Electron flow and biofilms. MRS Bull 36(5):380–384. doi:10.1557/mrs.2011.69

Neethirajan S, Karig D, Kumar A, Mukherjee PP, Retterer S, Doktycz M (2012) Biofilms in microfluidic devices. In: Bhushan B (ed) Encylopedia of nanotechnology. Springer, New York

Paramonova E, Kalmykowa OJ, van der Mei HC, Busscher HJ, Sharma PK (2009) Impact of hydrodynamics on oral biofilm strength. J Dent Res 88(10):922–926. doi:10.1177/0022034509344569

Park A, Jeong H–H, Lee J, Kim KP, Lee C-S (2011) Effect of shear stress on the formation of bacterial biofilm in a microfluidic channel. Biochip J 5(3):236–241. doi:10.1007/s13206-011-5307-9

Purevdorj B, Costerton JW, Stoodley P (2002) Influence of hydrodynamics and cell signaling on the structure and behavior of *Pseudomonas aeruginosa* biofilms. Appl Environ Microbiol 68(9):4457–4464. doi:10.1128/aem.68.9.4457-4464.2002

Qian F, Baum M, Gu Q, DE Morse (2009) A 1.5 μL microbial fuel cell for on-chip bioelectricity generation. Lab Chip 9(21):3076–3081. doi:10.1039/b910586g

Remis JP, Costerton JW, Auer M (2010) Biofilms: structures that may facilitate cell–cell interactions. ISME J 4(9):1085–1087. doi:10.1038/ismej.2010.105

Richter L, Stepper C, Mak A, Reinthaler A, Heer R, Kast M, Bruckl H, Ertl P (2007) Development of a microfluidic biochip for online monitoring of fungal biofilm dynamics. Lab Chip 7(12):1723–1731. doi:10.1039/b708236c

Rusconi R, Lecuyer S, Guglielmini L, Stone HA (2010) Laminar flow around corners triggers the formation of biofilm streamers. J R Soc Interface 7(50):1293–1299. doi:10.1098/rsif.2010.0096

Rusconi R, Lecuyer S, Autrusson N, Guglielmini L, Stone HA (2011) Secondary flow as a mechanism for the formation of biofilm streamers. Biophys J 100(6):1392–1399. doi:10.1016/j.bpj.2011.01.065

Santiago JG, Wereley ST, Meinhart CD, Beebe DJ, Adrian RJ (1998) A particle image velocimetry system for microfluidics. Exp Fluids 25(4):316–319

Shen C, Floryan JM (1985) Low Reynolds-number flow over cavities. Phys Fluids 28(11):3191–3202

Shrout JD, Tolker-Nielsen T, Givskov M, Parsek MR (2011) The contribution of cell–cell signaling and motility to bacterial biofilm formation. MRS Bull 36(5):367–373. doi:10.1557/mrs.2011.67

Stewart PS, Franklin MJ (2008) Physiological heterogeneity in biofilms. Nat Rev Microbiol 6(3):199–210. doi:10.1038/nrmicro1838

Stoodley P, Dodds I, Boyle JD, Lappin-Scott HM (1999) Influence of hydrodynamics and nutrients on biofilm structure. J Appl Microbiol 85:19S–28S

Thormann KM, Saville RM, Shukla S, Pelletier DA, Spormann AM (2004) Initial phases of biofilm formation in *Shewanella oneidensis* MR-1. J Bacteriol 186(23):8096–8104. doi:10.1128/jb.186.23.8096-8104.2004

Valiei A, Kumar A, Mukherjee PP, Liu Y, Thundat T (2012) A web of streamers: biofilm formation in a porous microfluidic device. Lab Chip 12(24):5133–5137

Volfson D, Cookson S, Hasty J, Tsimring LS (2008) Biomechanical ordering of dense cell populations. Proc Natl Acad Sci USA 105(40):15346–15351. doi:10.1073/pnas.0706805105

Wereley ST, Gui L, Meinhart CD (2002) Advanced algorithms for microscale particle image velocimetry. AIAA J 40(6):1047–1055

Wierschem A, Aksel N (2004) Influence of inertia on eddies created in films creeping over strongly undulated substrates. Phys Fluids 16(12):4566–4574. doi:10.1063/1.1811673

Wong GCL, O'Toole GA (2011) All together now: integrating biofilm research across disciplines. MRS Bull 36(5):339–345. doi:10.1557/mrs.2011.64

Yawata Y, Toda K, Setoyama E, Fukuda J, Suzuki H, Uchiyama H, Nomura N (2010) Bacterial growth monitoring in a microfluidic device by confocal reflection microscopy. J Biosci Bioeng 110(1):130–133. doi:10.1016/j.jbiosc.2010.01.009